# Improved particle swarm optimization algorithm and its application to search for new magnetic ground states in the Hubbard model

Ze Ruan,* Xiu-Cai Jiang,* Ze-Yi Song, and Yu-Zhong Zhang †

*Shanghai Key Laboratory of Special Artificial Microstructure Materials and Technology, School of Physics Science and Engineering, Tongji University, Shanghai 200092, China*

(Received 2 August 2023; revised 19 October 2023; accepted 6 December 2023; published 21 December 2023)

An improved particle swarm optimization algorithm is proposed, and its superiority over the standard particle swarm optimization algorithm is tested on two typical benchmark functions. By employing this algorithm to search for the magnetic ground states of the Hubbard model on the real-space square lattice with finite size based on the mean-field approximation, two new magnetic states, namely, the double-striped-type antiferromagnetic state and the triple antiferromagnetic state, are found. We further perform mean-field calculations in the thermodynamical limit to confirm that these two new magnetic states are not a result of a finite-size effect, where the properties of the double-striped-type antiferromagnetic state are also presented.

DOI: 10.1103/PhysRevResearch.5.043275

## I. INTRODUCTION

Antiferromagnetism has attracted tremendous interest due to the fact that the parent states of cuprates and iron-based superconductors are either antiferromagnets or paramagnets with antiferromagnetic fluctuations, such as the checkerboard antiferromagnetic (CAF) insulator of cuprates, nearly degenerate double-stripe (DAF) and plaquette antiferromagnetic (PAF) order in FeTe [1,2], pair-checkerboard antiferromagnetic (PCAF) order in monolayer FeSe thin film [3,4], molecular-intercalated FeSe [5], and $A_xFe_{2-y}Se_2$ [6], as well as stripe-type antiferromagnetic (SAF) order in other iron-based mother materials [7–9], which indicates a magnetic origin of the two high-$T_c$ unconventional superconductors.

Therefore much effort has been spent on studying the properties of these magnetic states based on models related to these two superconducting families. A simple Heisenberg model with the nearest- and next-nearest-neighbor intralayer couplings has been used to explain the transition from CAF to SAF [10]. Additionally, a combination of this simple Heisenberg model with the third-neighbor intralayer coupling solely [11,12], or with three couplings [13], namely, the third-neighbor intralayer coupling, nearest interlayer coupling, and intralayer nearest-neighbor biquadratic coupling, is introduced to further include DAF and PAF. In addition to these models, an effective orbital-degenerate double-exchange model consisting of both itinerant electrons and localized spins is used to take CAF, DAF, and SAF into consideration [14]. Alternatively, the Hubbard model, which covers both weak- and strong-coupling limits for magnetism, is also employed to investigate these magnetic states, for example, the single-orbital Hubbard model with the nearest- and next-nearest-neighbor hoppings. Using methods like variational cluster approximation (VCA) [15,16], variational Monte Carlo [17], and mean-field theory [18], the presence of CAF and SAF in this model is proposed. Apart from these two states, PCAF is also found in this model by the path-integral renormalization group method [19] and variational cluster approximation [20]. Recently it was pointed out that this Hubbard model can serve as a unified minimal model to describe all the magnetic states mentioned above [21].

However, despite numerous investigations, only a few new magnetic states which probably exist in the experiment are predicted based on the aforementioned superconductor-related magnetic models. For example, the spiral and staggered trimer states are predicted in the $J_1$-$J_2$-$J_3$-$K$ Heisenberg model [22], or a spiral state is found in a frustrated Hubbard model containing the nearest- and next-nearest-neighbor hoppings, where the latter hopping breaks $C_4$ symmetry [23]. The lack of new magnetic states may be due to the weakness of conventional methods, such as variational cluster approximation, variational Monte Carlo, mean-field theory, etc., as they require preparation of the desired configurations while it is impossible to exhaust all magnetic patterns. Thus a natural question arises regarding whether more new exotic magnetic states occur in the aforementioned unified minimal Hubbard model when a method superior to conventional methods is used. Noticeably, the particle swarm optimization (PSO) algorithm is proven to be a powerful approach [24,25], which is also used in the prediction of new materials [26–29] and the estimation of cosmological parameters [30,31], etc. Noting that PSO can handle problems with numerous energy minima [26] and generate random particles, it may be suitable to search for new magnetic states, where a magnetic pattern is viewed as a particle. Nevertheless, the insufficient

*These authors contributed equally to this paper.
†Corresponding author: yzzhang@tongji.edu.cn

*Published by the American Physical Society under the terms of the Creative Commons Attribution 4.0 International license. Further distribution of this work must maintain attribution to the author(s) and the published article's title, journal citation, and DOI.*

performance of standard PSO that sometimes converges slowly [32] or tends to converge to local minima [33] impedes such application. Although lots of attempts have been undertaken to improve the performance of the standard PSO [34–41], an improved PSO with the hyperparameters (including the inertial weight and learning factors) depending on the individual character of a particle has not yet been proposed. Therefore, proposing an improved PSO with particle-dependent hyperparameters and using it to search for new magnetic states in the aforementioned Hubbard model is an interesting work.

In this paper we propose an improved PSO where the hyperparameters of a specific particle depend on its present position, corresponding local best, and global best. We first show the superiority of this improved PSO over standard PSO on two typical benchmark functions, namely, the Griewank function and Rastrigin function. Then, by employing this improved PSO to search for the magnetic ground state of the Hubbard model on the real-space square lattice with a finite size of $24 \times 24$ based on the mean-field approximation, two new magnetic states are found, namely, the double-striped-type state (DSAF) and the triple antiferromagnetic state (TAF). By comparing the free energies of these two new states with their competing states in corresponding parameter space using mean-field theory in the thermodynamical limit, we further confirm that these two new magnetic states are not a result of a finite-size effect. In addition, we present the properties of the DSAF, which occurs at a region of weak frustration.

Our paper is organized as follows. Section II describes the Hubbard model and the standard PSO. Section III presents our main results, including the superiority of our improved PSO over the standard PSO, the search of new magnetic ground states of the Hubbard model on the square lattice with a finite real-space size using improved PSO, and the mean-field calculations in the thermodynamical limit. Section IV presents a detailed discussion, and Sec. V concludes with a summary.

## II. MODEL AND METHOD

The Hubbard model on a square lattice with the nearest- and next-nearest-neighbor hoppings we studied is given by

$$H = -t_1 \sum_{\langle i,j\rangle,\sigma} c_{i\sigma}^{\dagger} c_{j\sigma} - t_2 \sum_{\langle\langle i,j\rangle\rangle,\sigma} c_{i\sigma}^{\dagger} c_{j\sigma} + U \sum_i n_{i\uparrow} n_{i\downarrow}, \quad (1)$$

where $c_{i\sigma}^{\dagger}(c_{i\sigma})$ creates (annihilates) an electron at site $i$ with spin $\sigma$, $n_{i\sigma}$ is the number operator, $t_1$ and $t_2$ denote the nearest- and next-nearest-neighbor hoppings, and $U$ is the onsite Coulomb interaction. $\langle i,j\rangle(\langle\langle i,j\rangle\rangle)$ means the summation over nearest (next-nearest)-neighbor sites. The on-site Coulomb interaction is treated by the mean-field approximation as

$$U n_{i\uparrow} n_{i\downarrow} \approx U n_{i\uparrow}\langle n_{i\downarrow}\rangle + U\langle n_{i\uparrow}\rangle n_{i\downarrow} - U\langle n_{i\uparrow}\rangle\langle n_{i\downarrow}\rangle. \quad (2)$$

By respectively defining the magnetic moment and charge occupation of site $i$ as $m_i = \langle n_{i\uparrow}\rangle - \langle n_{i\downarrow}\rangle$ and $\bar{n}_i = \langle n_{i\uparrow}\rangle + \langle n_{i\downarrow}\rangle$, we have

$$\langle n_{i\uparrow}\rangle = \tfrac{1}{2}(\bar{n}_i + m_i), \quad \langle n_{i\downarrow}\rangle = \tfrac{1}{2}(\bar{n}_i - m_i). \quad (3)$$

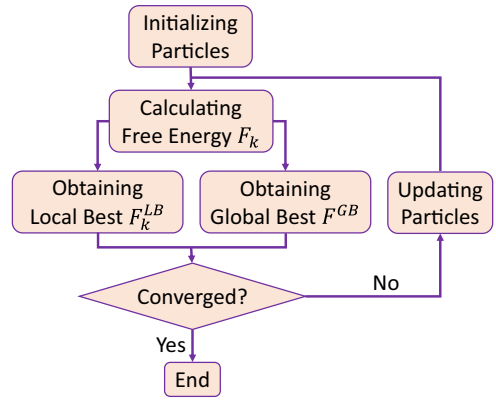


FIG. 1. The flowchart of PSO, where local best and global best are the minimal free energy of the $k$th particle and all particles, respectively. When the convergence criterion is reached, $|F_k^{\rm LB} - F^{\rm GB}| < \epsilon$ satisfies for any given $k$th particle, where $\epsilon$ is a small positive number.

Thus, for a given charge distribution and magnetic configuration $\{\bar{n}_1, \ldots, \bar{n}_N, m_1, \ldots, m_N\}$, the free energy can be calculated as

$$F = -\frac{1}{\beta}\ln\Xi + \sum_{\rm i=1}^{\rm N}\left(\mu + \frac{Um_i^2}{4} - \frac{U\bar{n}_i^2}{4}\right), \quad (4)$$

in which the grand partition function reads

$$\ln\Xi = \sum_{\sigma}\sum_{\rm i=1}^{\rm N}\ln[1 + {\rm e}^{-\beta(E_{i\sigma}-\mu)}], \quad (5)$$

where $N$ is the total number of sites in the system, $\beta$ is the inverse temperature defined as $1/(k_B T)$, $\mu$ denotes the chemical potential, and $E_{i\sigma}$ is the eigenvalue derived by diagonalizing the Hamiltonian matrix of the system. Specifically, for the case with uniform charge distribution at half-filling, namely, $\bar{n}_1 = \cdots = \bar{n}_N = 1$, the free energy is a function of the magnetic configuration $\{m_1, \ldots, m_N\}$. We proceed to demonstrate how this Hubbard model is solved within the framework of PSO based on the mean-field approximation, where a magnetic configuration is viewed as a particle and free energy $F$ is the target function to be optimized to a minimum value. The flowchart of PSO is shown in Fig. 1. As can be seen, the first iteration consists of the following four steps, while the other iterations contain the last three of these steps within the framework of PSO:

(i) Initializing random particles, namely, a set of magnetic configurations $\{X_1, \ldots, X_k, \ldots, X_P\}$, where $X_k = \{m_1^k, \ldots, m_N^k\}$, and $P$ is the total number of particles.

(ii) Calculating the free energies of these magnetic configurations $\{F_1, \ldots, F_k, \ldots, F_P\}$ according to Eq. (4).

(iii) Evaluating local best $\{F_1^{\rm LB}, \ldots, F_k^{\rm LB}, \ldots, F_P^{\rm LB}\}$ and global best $F^{\rm GB}$ based on $\{F_1, \ldots, F_k, \ldots, F_P\}$ of the current and last iterations.

(iv) Determining whether the convergence criterion is reached. If $|F_k^{\rm LB} - F^{\rm GB}| < \epsilon$ satisfies for any given $k$th particle, where $\epsilon$ is a small positive number, the calculation is completed; otherwise, updating the magnetic configurations

and turning to step (ii) using the following equations:

$$D_k^{\mathrm{New}} = \omega D_k^{\mathrm{Old}} + c_1 r_1 \left(X_k^{\mathrm{LB}} - X_k\right) + c_2 r_2 (X^{\mathrm{GB}} - X_k),$$
$$X_k^{\mathrm{New}} = X_k + D_k^{\mathrm{New}}, \tag{6}$$

where $\omega$ denotes the inertial weight, $c_1$ and $c_2$ are the learning factors, and $r_1(r_2)$ is a random number between 0 and 1 that varies at each iteration. $X_k^{\mathrm{LB}}$ and $X^{\mathrm{GB}}$ are the magnetic configurations of local best and global best, respectively. $D_k^{\mathrm{New}}$ and $D_k^{\mathrm{Old}}$ denote separately the displacement between the new and current $k$th magnetic configurations and that between the current and last $k$th magnetic configurations, in which $D_k^{\mathrm{Old}}$ should be initialized at the first iteration. It is necessary to mention that, for standard PSO, $c_1$, $c_2$, and $\omega$ are particle-independent, where $c_1$ and $c_2$ are two constants while $\omega$ decreases linearly at first and then remains a small value the iteration proceeds.

In contrast to standard PSO, the learning factors and inertial weight of our improved PSO are particle dependent, where $c_1$ and $c_2$ have the forms

$$c_{1k} = \frac{e^{F^{\mathrm{GB}}}}{e^{F^{\mathrm{GB}}} + e^{F_k^{\mathrm{LB}}}}, \quad c_{2k} = \frac{e^{F_k^{\mathrm{LB}}}}{e^{F^{\mathrm{GB}}} + e^{F_k^{\mathrm{LB}}}}, \tag{7}$$

while $\omega$ reads

$$\omega_k = \begin{cases} \xi & \left(F_k \leqslant F^{\mathrm{GB}} \cap F_k \leqslant F_k^{\mathrm{LB}}\right) \\ (F_k - F^{\mathrm{GB}})^{\gamma} & \left(F^{\mathrm{GB}} < F_k < F_k^{\mathrm{LB}}\right) \\ \left(2F_k - F^{\mathrm{GB}} - F_k^{\mathrm{LB}}\right)^{\gamma} & \left(F^{\mathrm{GB}} < F_k \cap F_k^{\mathrm{LB}} < F_k\right) \end{cases}, \tag{8}$$

in which $\gamma$ is a tunable positive number with the highest performance when $1.5 \sim 1.7$ for the Rastrigin function, $5 \sim 7$ for the Griewank function, and 0.01 for this Hubbard model, while $\xi$ is a small positive number. Thus, by combining Eqs. (4)–(8), the Hubbard model can be solved self-consistently using our improved PSO.

## III. RESULTS

### A. The superiority of our improved PSO over standard PSO

We will now investigate the superiority of our improved PSO over standard PSO on two typical benchmark functions, namely, the Griewank function and Rastrigin function. As we have proposed the improved version for both the learning factors and inertial weight in our improved PSO, it is necessary to use the controlled variable method to separately investigate the performance improvement for standard PSO when including the learning factors or inertial weight individually.

In Fig. 2 we compare the convergence process on the Griewank function [Fig. 2(a)] and Rastrigin function [Fig. 2(b)] using PSO with improved $c_1$ and $c_2$ or with standard $c_1$ and $c_2$, where the inertial weight of standard PSO is used. Obviously, for these two typical benchmark functions, the convergence process of PSO using our improved version of $c_1$ and $c_2$ converges faster than that using $c_1$ and $c_2$ of the standard PSO in a wide range of parameter space, indicating the superiority of our improved PSO over the standard PSO regarding the learning factors.

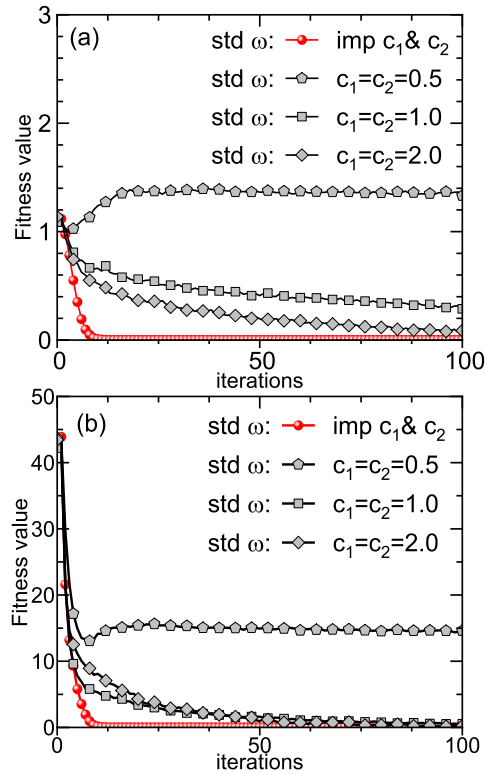


FIG. 2. The convergence process on the Griewank function (a) and Rastrigin function (b) using PSO with improved $c_1$ and $c_2$ or with standard $c_1$ and $c_2$, where the inertial weight ($\omega$) of standard PSO is used.

Furthermore, we compare the convergence process on the Griewank function and Rastrigin function in Figs. 3(a) and 3(b), respectively, using PSO with the improved version of $\omega$ or with the standard version of $\omega$, where the learning factors of standard PSO are used. Similarly, our improved version of $\omega$ exhibits higher performance than the standard version of $\omega$ in wide range of $c_1$ and $c_2$ for these two typical benchmark functions.

Thus, for both learning factors and inertial weight, our improved versions exhibit a higher performance than the standard PSO. It is necessary to mention that the combination of these two kinds of improved hyperparameters converges faster than the inclusion of learning factors or inertial weight individually.

### B. The application of improved PSO in the Hubbard model

We now employ our improved PSO to search for new magnetic ground states of the Hubbard model on the real-space square lattice with a finite size of $24 \times 24$ based on the mean-field approximation. The periodic boundary condition is used. Since particles, namely, the magnetic configurations, will ultimately converge to the position where the free energy is minimized, regardless of their initial positions within the framework of this algorithm, we initialize the magnetic configurations randomly and update them iteratively following the flowchart as shown in Fig. 1. Notably, two new magnetic states, namely, DSAF and TAF, are found apart from the existing states of CAF, DAF, PAF, PCAF, and SAF,

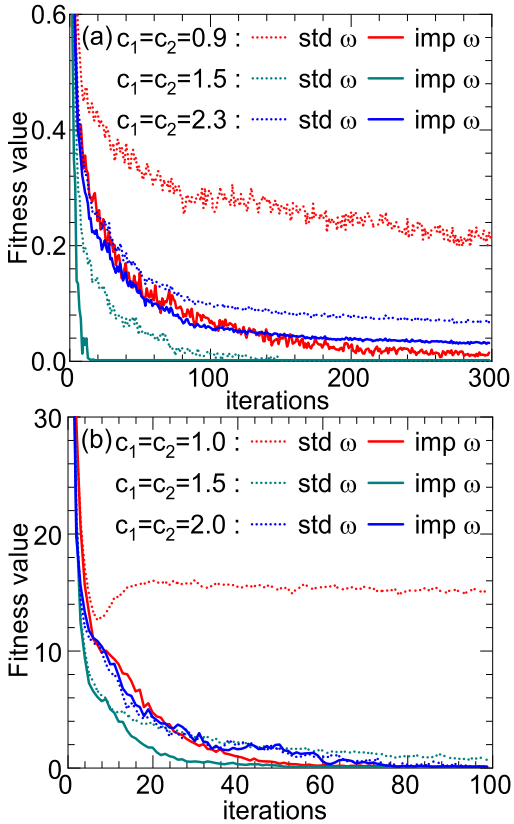


FIG. 3. The convergence process on the Griewank function (a) and Rastrigin function (b) using PSO with improved $\omega$ or with standard $\omega$ where the learning factors ($c_1$ and $c_2$) of the standard PSO are used.

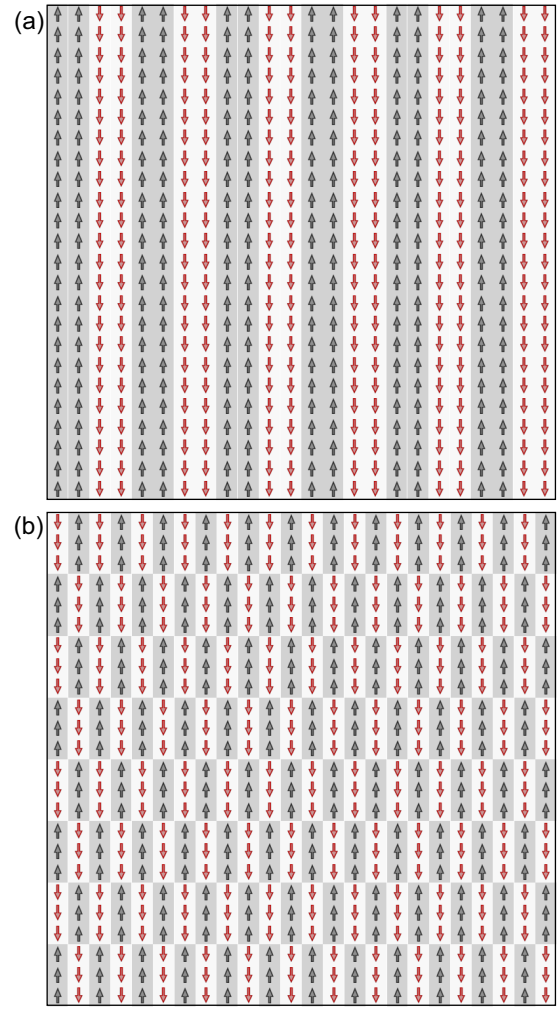


FIG. 4. The DSAF and TAF patterns found by our improved PSO on the real-space square lattice with a finite size of $24 \times 24$, where $t_2/t_1 = 0.99$ and $U/t_1 = 3.4$ in (a), while $t_2/t_1 = 0.765$ and $U/t_1 = 4.43$ in (b).

where DSAF is in the region of weak geometrical frustration, while TAF is located in the strong geometrical frustration region. Interestingly, a Hubbard model with only the nearest- and next-nearest-neighbor hoppings can favor TAF, whereas $J_1$, $J_2$, $J_3$, and $K$ are needed for a Heisenberg model [22]. The specific configurations of DSAF and TAF are shown in Figs. 4(a) and 4(b), respectively. It is necessary to mention that the calculations here are performed on a finite size of only $24 \times 24$, which may be affected by finite-size effects.

To confirm that these two new magnetic states are not a result of a finite-size effect, we further perform mean-field calculations in the thermodynamical limit. Figure 5 shows the comparison of free energies between DSAF and its corresponding competing states 5(a), as well as between TAF and its corresponding competing states 5(b). Obviously, DSAF occurs in the region between the paramagnetic state (PM) and SAF, while TAF exists in the region between PAF and PCAF. Thus the presence of our two new magnetic states is confirmed in the thermodynamical limit, which is not a result of a finite-size effect.

Considering that DSAF occurs at $2.8 < U/t_1 < 4.5$ ($0.23 < U/W < 0.36$, where $W$ is the bandwidth) for $t_2/t_1 = 0.99$, where geometrical frustration is released and the electronic correlation is relatively weak, this state may be reliable within the mean-field approximation. Thus we investigate the band structure and density of states (DOS) for DSAF in Fig. 6. As can be seen, DSAF is metallic. Furthermore, we demonstrate the magnetic moments of DSAF and its corresponding competing states as a function of the on-site Coulomb interaction $U$ at $t_2/t_1 = 0.99$ in Fig. 7(a). The sudden enhancements of the magnetic moments from PM to DSAF and from DSAF to SAF suggest first-order phase transitions. The kink occurring in the magnetic moment for the case of SAF is a result of a phase transition from metallic SAF to insulating SAF, consistent with a previous study [18]. We also present a schematic phase diagram of DSAF in Fig. 7(b). Obviously, DSAF becomes the ground state within a broad region for the magnetic states we considered.

## IV. DISCUSSION

We have proposed an idea about how to search for magnetic ground states of the Hubbard model using PSO based on the mean-field approximation by viewing magnetic configurations as particles. We have found two new magnetic ground states in the Hubbard model with the nearest- and

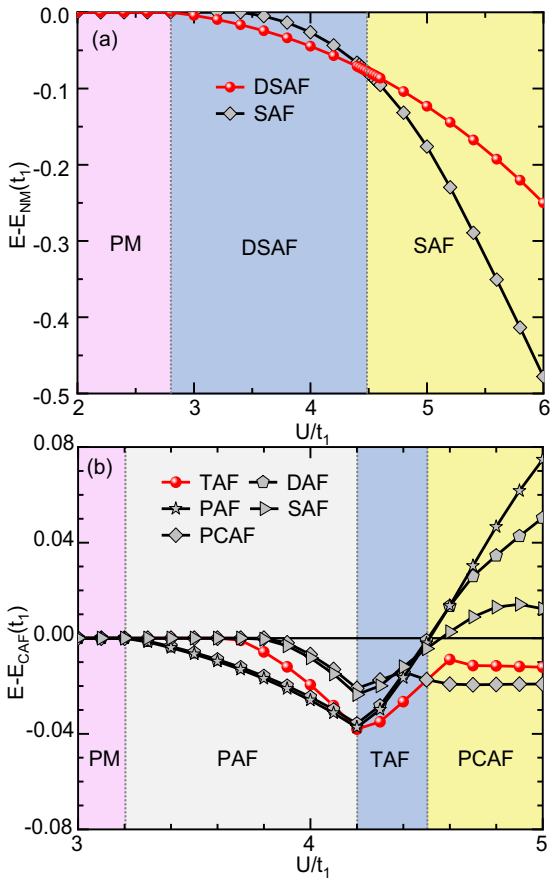


FIG. 5. (a) The free energies of SAF and DSAF as functions of the on-site Coulomb interaction $U$ at $t_2/t_1 = 0.99$, where the energy of the paramagnetic state is set to zero. (b) The free energies of CAF, DAF, TAF, PCAF, PAF, and SAF as functions of U at $t_2/t_1 = 0.765$, where the energy of the paramagnetic state is set to zero.

next-nearest-neighbor hoppings by employing our improved version of PSO. Although the PSO calculations in this paper are based on the mean-field approximation, PSO is a very powerful algorithm that can be effectively combined with higher-level approximations to handle the Hubbard model, such as the Hubbard-I approximation [42], Hubbard-III approximation [43], the projective operator approximation [44,45], coherent potential approximation [46–48], dynamical mean-field theory [49,50], etc.

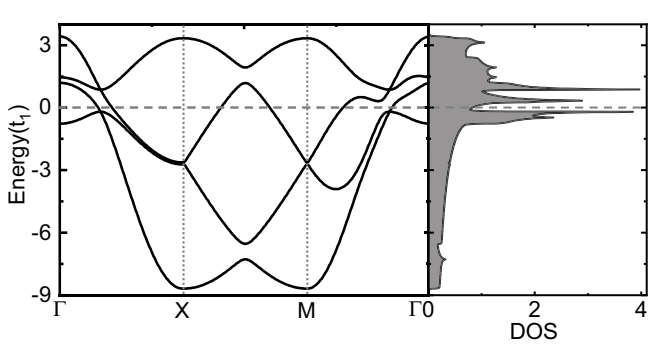


FIG. 6. Band structure and corresponding DOS for the DSAF state at $t_2/t_1 = 0.99$ and $U/t_1 = 3.6$.

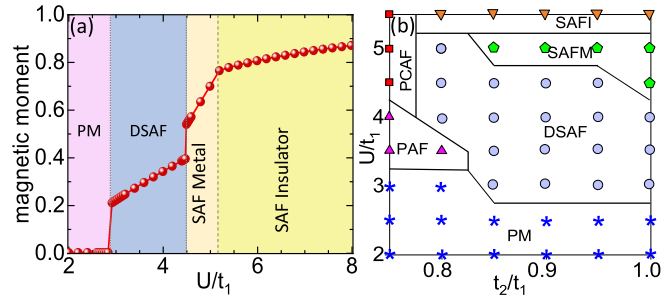


FIG. 7. (a) The magnetic moment as a function of the on-site Coulomb interaction $U$ at $t_2/t_1 = 0.99$. (b) A schematic phase diagram in the region of $0.75 < t_2/t_1 < 1$ and $2 < U/t_1 < 5.5$, in which the star, square, triangle, inverted triangle, pentagon, and circle denote PM, PCAF, PAF, SAF insulator (SAFI), SAF metal (SAFM), and DSAF, respectively.

Twisting often leads to the emergence of exotic magnetic phases in layered materials, such as the coexistence of interlayer ferromagnetic and interlayer antiferromagnetic states in twisted bilayer $CrI_3$ [51]. However, enumerating all the possible magnetic states in twisted layered materials becomes challenging due to the large number of sublattices in the supercell. Fortunately, PSO offers an excellent platform to automatically search for the magnetic ground state without the need for manual preparation of magnetic configurations. Therefore the application of PSO in studying the magnetism of twisted systems is expected to be very interesting.

By using PSO we have discovered two new magnetic states in the Hubbard model we investigated, including DSAF and TAF. Although a double-Q coplanar spin-vortex crystal phase is proposed when $t_2 \approx t_1$ and $U/W > 0.31$ ($U/t_1 > 3.8$) [52], our DSAF occurs at the region with a weaker correlation interaction of $U/W > 0.23$ ($U/t_1 > 2.8$). Besides, since the geometrical frustration is released and the electronic correlation is weak, the mean-field approximation is reliable, as evidenced by qualitative consistencies between solutions from the mean-field approximation [21] and VCA [16], where SAF starts to appear at $U/t_1$ less than 4 if DSAF is not taken into account, indicating that quantum fluctuations completely ignored in the mean-field approximation are suppressed in the large $t_2/t_1$ and weak $U/W$ region.. Since the free energy of DSAF is significantly lower than that of other states in the DSAF phase, it is reasonably expected that the stable DSAF solution should survive against the quantum fluctuations, due to the fact that even the metastable SAF solution has already survived against the quantum fluctuations [16]. Additionally, we find that a prominent peak is present in the vicinity of $(\pi/2, 0)$ for the Pauli susceptibility in the $t_2 \approx t_1$ region, indicating a tendency towards DSAF if perturbation, like the on-site Coulomb interaction, is switched on, further supporting our finding of DSAF in a particular region. Thus DSAF is most probably a genuine ground state in a sufficient large parameter space for this Hubbard model, even if both noncollinear magnetism and quantum fluctuations are considered. In contrast, TAF may be controversial since it occurs in the region of strong geometric frustration, where macroscopic degeneracies dramatically affect the magnetism of the

one-band Hubbard model. As a result, various competing states are proposed in this region, such as PCAF [19,20], DAF [21], PAF [21], as well as nonmagnetic insulating states [19]. Thus it is interesting to use a more sophisticate method than the mean-field approximation to confirm the stability of TAF over its corresponding competing states.

Compared to standard PSO, our improved PSO exhibits a higher performance because the search direction of particles in the standard PSO is so random that it lacks sufficient guidance. In contrast, by proposing an improved version of the learning factors and inertial weight, particles have their own characteristics to recognize the searching direction in our improved PSO, which significantly saves the time of particles wandering around a local optimum. Thus, our improved PSO converges faster than standard PSO. Our work provides valuable insights into how to improve PSO by modifying the learning factors and inertial weight and demonstrates its effectiveness in searching new states of matter.

## V. CONCLUSION

In conclusion, we have proposed an improved version of PSO that converges to the global optimum faster than standard PSO. By employing this improved PSO to search for new magnetic states in the Hubbard model with the nearest- and next-nearest-neighbor hoppings on a real-space square lattice with a finite size of $24 \times 24$ based on the mean-field approximation, two new magnetic states, including DSAF and TAF, are found. The presence of these two states in this Hubbard model is further confirmed by mean-field calculations in the thermodynamical limit, where the band structure, DOS, and magnetic moment of DSAF are also present.

## ACKNOWLEDGMENTS

This work is supported by the National Natural Science Foundation of China (Grants No. 12274324 and No. 12004283) and Shanghai Science and Technology Commission (Grant No. 21JC405700).

[1] S. Li, C. de la Cruz, Q. Huang, Y. Chen, J. W. Lynn, J. Hu, Y.-L. Huang, F.-C. Hsu, K.-W. Yeh, M.-K. Wu, and P. Dai, First-order magnetic and structural phase transitions in $Fe_{1+y}Se_xTe_{1-x}$, Phys. Rev. B **79**, 054503 (2009).

[2] D. W. Tam, H. H. Lai, J. Hu, X. Lu, H. C. Walker, D. L. Abernathy, J. L. Niedziela, T. Weber, M. Enderle, Y. Su, Z. Q. Mao, Q. Si, and P. Dai, Plaquette instability competing with bicollinear ground state in detwinned FeTe, Phys. Rev. B **100**, 054405 (2019).

[3] Y. Zhou, L. Miao, P. Wang, F. F. Zhu, W. X. Jiang, S. W. Jiang, Y. Zhang, B. Lei, X. H. Chen, H. F. Ding *et al.*, Antiferromagnetic order in epitaxial FeSe films on $SrTiO_3$, Phys. Rev. Lett. **120**, 097001 (2018).

[4] H.-Y. Cao, S. Chen, H. Xiang, and X.-G. Gong, Antiferromagnetic ground state with pair-checkerboard order in FeSe, Phys. Rev. B **91**, 020504(R) (2015).

[5] A. E. Taylor, S. J. Sedlmaier, S. J. Sedlmaier, S. J. Cassidy, E. A. Goremychkin, R. A. Ewings, T. G. Perring, S. J. Clarke, and A. T. Boothroyd, Spin fluctuations away from $(\pi, 0)$ in the superconducting phase of molecular-intercalated FeSe, Phys. Rev. B **87**, 220508(R) (2013).

[6] A. E. Taylor, R. A. Ewings, T. G. Perring, J. S. White, P. Babkevich, A. Krzton-Maziopa, E. Pomjakushina, K. Conder, and A. T. Boothroyd, Spin-wave excitations and superconducting resonant mode in $Cs_xFe_{2-y}Se_2$, Phys. Rev. B **86**, 094528 (2012).

[7] C. dé La Cruz, Q. Huang, J. W. Lynn, J. Li, W. R. Ii, J. L. Zarestky, H. A. Mook, G. F. Chen, J. L. Luo, N. L. Wang *et al.*, Magnetic order close to superconductivity in the iron-based layered $LaO_{1-x}F_xFeAs$ systems, Nature (London) **453**, 899 (2008).

[8] Q. Huang, Y. Qiu, W. Bao, M. A. Green, J. W. Lynn, Y. C. Gasparovic, T. Wu, G. Wu, and X. H. Chen, Neutron-diffraction measurements of magnetic order and a structural transition in the parent $BaFe_2As_2$ compound of FeAs-based high-temperature superconductors, Phys. Rev. Lett. **101**, 257003 (2008).

[9] S. Li, C. de La Cruz, Q. Huang, G. F. Chen, T. L. Xia, J. L. Luo, N. L. Wang, and P. Dai, Structural and magnetic phase transitions in $Na_{1-\delta}FeAs$, Phys. Rev. B **80**, 020504(R) (2009).

[10] P. Chandra, P. Coleman, and A. I. Larkin, Ising transition in frustrated Heisenberg models, Phys. Rev. Lett. **64**, 88 (1990).

[11] F. Ma, W. Ji, J. Hu, Z.-Y. Lu, and T. Xiang, First-principles calculations of the electronic structure of tetragonal $\alpha$-FeTe and $\alpha$-FeSe crystals: Evidence for a bicollinear antiferromagnetic order, Phys. Rev. Lett. **102**, 177003 (2009).

[12] S. Ducatman, N. B. Perkins, and A. Chubukov, Magnetism in parent iron chalcogenides: Quantum fluctuations select plaquette order, Phys. Rev. Lett. **109**, 157206 (2012).

[13] J. Hu, B. Xu, W. Liu, N.-N. Hao, and Y. Wang, Unified minimum effective model of magnetic properties of iron-based superconductors, Phys. Rev. B **85**, 144403 (2012).

[14] W.-G. Yin, C.-C. Lee, and W. Ku, Unified picture for magnetic correlations in iron-based superconductors, Phys. Rev. Lett. **105**, 107004 (2010).

[15] S. Yamaki, K. Seki, and Y. Ohta, Ground-state phase diagram of the asymmetric Hubbard model with geometrical frustration, Phys. Rev. B **87**, 125112 (2013).

[16] A. H. Nevidomskyy, C. Scheiber, D. Sénéchal, and A. M. S. Tremblay, Magnetism and d-wave superconductivity on the half-filled square lattice with frustration, Phys. Rev. B **77**, 064427 (2008).

[17] L. F. Tocchio, F. Becca, A. Parola, and S. Sorella, Role of backflow correlations for the nonmagnetic phase of the $t$–$t'$ Hubbard model, Phys. Rev. B **78**, 041101(R) (2008).

[18] Z.-Q. Yu and L. Yin, Collinear antiferromagnetic state in a two-dimensional Hubbard model at half filling, Phys. Rev. B **81**, 195122 (2010).

[19] T. Mizusaki and M. Imada, Gapless quantum spin liquid, stripe, and antiferromagnetic phases in frustrated Hubbard models in two dimensions, Phys. Rev. B **74**, 014421 (2006).

[20] A. Yamada, K. Seki, R. Eder, and Y. Ohta, Magnetic properties and Mott transition in the square-lattice Hubbard model with frustration, Phys. Rev. B **88**, 075114 (2013).

[21] Z. Ruan, X.-C. Jiang, Z.-Y. Song, and Y.-Z. Zhang, Uncovering double-stripe and plaquette antiferromagnetic states in the one-band Hubbard model on a frustrated square lattice, New J. Phys. **23**, 053028 (2021).

[22] J. K. Glasbrenner, I. I. Mazin, H. O. Jeschke, P. J. Hirschfeld, R. M. Fernandes, and R. Valentí, Effect of magnetic frustration on nematicity and superconductivity in iron chalcogenides, Nat. Phys. **11**, 953 (2015).

[23] K. Misumi, T. Kaneko, and Y. Ohta, Phase diagram of the frustrated square-lattice Hubbard model: Variational cluster approach, J. Phys. Soc. Jpn. **85**, 064711 (2016).

[24] J. Kennedy and R. Eberhart, Particle swarm optimization, in *Proceedings of the ICNN'95-International Conference on Neural Networks* (IEEE, New York, 1995), Vol. 4, pp. 1942–1948.

[25] R. Eberhart and J. Kennedy, A new optimizer using particle swarm theory, in *MHS'95. Proceedings of the Sixth International Symposium on Micro Machine and Human Science* (IEEE, New York, 1995), pp. 39–43.

[26] Y. Wang, J. Lv, L. Zhu, and Y. Ma, Crystal structure prediction via particle-swarm optimization, Phys. Rev. B **82**, 094116 (2010).

[27] S. Zhang, Y. Li, T. Zhao, and Q. Wang, Robust ferromagnetism in monolayer chromium nitride, Sci. Rep. **4**, 5241 (2014).

[28] X. Qu, L. Yang, J. Lv, Y. Xie, J. Yang, Y. Zhang, Y. Wang, J. Zhao, Z. Chen, and Y. Ma, Particle swarm predictions of a $SrB_8$ monolayer with 12-fold metal coordination, J. Am. Chem. Soc. **144**, 11120 (2022).

[29] S. Yan, Y. Liu, Z. Wang, X. Lan, Y. Wang, and J. Ren, Designing radiative cooling metamaterials for passive thermal management by particle swarm optimization, Chin. Phys. B **32**, 057802 (2023).

[30] J. Prasad and T. Souradeep, Cosmological parameter estimation using particle swarm optimization, Phys. Rev. D **85**, 123008 (2012).

[31] A. N. Ruiz, S. A Cora, N. D. Padilla, M. J. Domínguez, C. A. Vega-Martínez, T. E Tecce, Á. Orsi, Y. Yaryura, D. G. Lambas, I. D. Gargiulo *et al.*, Calibration of semi-analytic models of galaxy formation using particle swarm optimization, Astrophys. J. **801**, 139 (2015).

[32] Z. Beheshti and S. M. H. Shamsuddin, CAPSO: Centripetal accelerated particle swarm optimization, Inf. Sci. **258**, 54 (2014).

[33] M. Clerc and J. Kennedy, The particle swarm-explosion, stability, and convergence in a multidimensional complex space, IEEE Trans. Evol. Comput. **6**, 58 (2002).

[34] R. Mendes, J. Kennedy, and J. Neves, The fully informed particle swarm: Simpler, maybe better, IEEE Trans. Evol. Comput. **8**, 204 (2004).

[35] A. Chatterjee and P. Siarry, Nonlinear inertia weight variation for dynamic adaptation in particle swarm optimization, Comput. Oper. Res. **33**, 859 (2006).

[36] Y. Wang, B. Li, T. Weise, J. Wang, B. Yuan, and Q. Tian, Self-adaptive learning based particle swarm optimization, Inf. Sci. **181**, 4515 (2011).

[37] A. Engelbrecht, Particle swarm optimization: Velocity initialization, in *2012 IEEE Congress on Evolutionary Computation* (IEEE, New York, 2012), pp. 1–8.

[38] Y. Li, Z.-H. Zhan, S. Lin, J. Zhang, and X. Luo, Competitive and cooperative particle swarm optimization with information sharing mechanism for global optimization problems, Inf. Sci. **293**, 370 (2015).

[39] M. Munlin and M. Anantathanavit, New social-based radius particle swarm optimization, in *Proceedings of the 2017 12th IEEE Conference on Industrial Electronics and Applications (ICIEA)* (IEEE, New York, 2017), pp. 838–843.

[40] J. Wu, C. Song, C. Fan, A. Hawbani, L. Zhao, and X. Sun, DENPSO: A distance evolution nonlinear PSO algorithm for energy-efficient path planning in 3D UASNs, IEEE Access **7**, 105514 (2019).

[41] J. Jakubik, A. Binding, and S. Feuerriegel, Directed particle swarm optimization with Gaussian-process-based function forecasting, Eur. J. Oper. Res. **295**, 157 (2021).

[42] J. Hubbard, Electron correlations in narrow energy bands, Proc. R. Soc. London, Ser. A **276**, 238 (1963).

[43] J. Hubbard, Electron correlations in narrow energy bands. III. An improved solution, Proc. R. Soc. London, Ser. A **281**, 401 (1964).

[44] L. M. Roth, Electron correlation in narrow energy bands. I. The two-pole approximation in a narrow *S* band, Phys. Rev. **184**, 451 (1969).

[45] P. Fan, K. Yang, K.-H. Ma, and N.-H. Tong, Projective truncation approximation for equations of motion of two-time Green's functions, Phys. Rev. B **97**, 165140 (2018).

[46] P. Soven, Coherent-potential model of substitutional disordered alloys, Phys. Rev. **156**, 809 (1967).

[47] B. Velický, S. Kirkpatrick, and H. Ehrenreich, Single-site approximations in the electronic theory of simple binary alloys, Phys. Rev. **175**, 747 (1968).

[48] J.-R. Xu, Z.-Y. Song, H.-Q. Lin, and Y.-Z. Zhang, Gate-induced gap in bilayer graphene suppressed by Coulomb repulsion, Phys. Rev. B **93**, 035109 (2016).

[49] A. Georges and G. Kotliar, Hubbard model in infinite dimensions, Phys. Rev. B **45**, 6479 (1992).

[50] A. Georges, G. Kotliar, W. Krauth, and M. J. Rozenberg, Dynamical mean-field theory of strongly correlated fermion systems and the limit of infinite dimensions, Rev. Mod. Phys. **68**, 13 (1996).

[51] Y. Xu, A. Ray, Y.-T. Shao, S. Jiang, K. Lee, D. Weber, J. E. Goldberger, K. Watanabe, T. Taniguchi, D. A. Muller *et al.*, Coexisting ferromagnetic–antiferromagnetic state in twisted bilayer $CrI_3$, Nat. Nanotechnol. **17**, 143 (2022).

[52] Y.-P. Huang, J.-W. Dong, P. Kotetes, and S. Zhou, Antiferromagnetic chiral spin density wave and strain-induced Chern insulator in the square lattice Hubbard model with frustration, Phys. Rev. B **102**, 195120 (2020).